Neuron
Article

Membrane Potential Synchrony in Primary Visual Cortex during Sensory Stimulation

Jianing Yu[1,2] and David Ferster[1,2,*]
[1]Department of Neurobiology and Physiology
[2]Interdepartmental Neuroscience Program
Northwestern University, Evanston, IL 60208, USA
*Correspondence: ferster@northwestern.edu
DOI 10.1016/j.neuron.2010.11.027

SUMMARY

When the primary visual cortex (V1) is activated by sensory stimulation, what is the temporal correlation between the synaptic inputs to nearby neurons? This question underlies the origin of correlated activity, the mechanism of how visually evoked activity emerges and propagates in cortical circuits, and the relationship between spontaneous and evoked activity. Here, we have recorded membrane potential from pairs of V1 neurons in anesthetized cats and found that visual stimulation suppressed low-frequency membrane potential synchrony (0–10 Hz), and often increased synchrony at high frequencies (20–80 Hz). The increase in high-frequency synchrony occurred for neurons with similar orientation preferences and for neurons with different orientation preferences and occurred for a wide range of stimulus orientations. Thus, while only a subset of neurons spike in response to visual stimulation, a far larger proportion of the circuit is correlated with spiking activity through subthreshold, high-frequency synchronous activity that crosses functional domains.

INTRODUCTION

It has often been proposed that the precise timing and correlation of neuronal activity is as much a part of the neural code as the spatial distribution of spike rate activity in the population (deCharms and Zador, 2000; Tiesinga et al., 2008). In primary visual cortex, as well as in other sensory or nonsensory cortices, spike activity of single neurons is often temporally correlated on a millisecond time scale with that of other neurons or with the ensemble activity of the local population (deCharms and Merzenich, 1996; Gray et al., 1989; Gray and Singer, 1989; Kohn and Smith, 2005; Murthy and Fetz, 1996; Pesaran et al., 2002; Ts'o et al., 1986; Tsodyks et al., 1999). This sharp correlation reflects a correlation of presynaptic inputs to a population of neurons. One way to begin to unravel the correlation is to measure and compare the membrane potential (V_m) activity of pairs of cells (Gentet et al., 2010; Lampl et al., 1999; Poulet and Petersen, 2008; Volgushev et al., 2006). Based on pairwise correlation analysis, one may be able to infer the correlation structure for a large population.

In primary visual cortex, the synchronization of spontaneous V_m fluctuations has been studied in detail (Lampl et al., 1999). Visual stimulation, however, clearly reorganizes the activity of V1 circuits by preferentially activating neurons that represent the visual features of the stimulus. During visual stimulation, V_m fluctuations of single V1 neurons exhibit a variety of temporal patterns (Bringuier et al., 1997; Jagadeesh et al., 1992), often including a significant increase in the amplitude of high-frequency components, which control the timing of spikes (Azouz and Gray, 2000, 2003). The correlation of these visually evoked high-frequency fluctuations between nearby V1 neurons has only been examined for a limited number of cells and visual stimuli (Lampl et al., 1999). Here, using dual whole-cell patch recordings in vivo, we have characterized the dependence of V_m correlation on the stimulus parameters and on the functional specificity of neurons.

We have asked the following questions. First, are neurons in different functional domains constrained from interacting with each other during visual stimulation? That is, does the V_m correlation during visual stimulation depend on the difference in tuning properties between neurons? Given the intricate architecture of cortical circuits (e.g., Ohki et al., 2006; Ohki and Reid, 2007; Song et al., 2005; Yoshimura et al., 2005), it is possible that neurons' V_m activity can be synchronized or desynchronized during visual stimulation depending on their functional specificity and the visual stimulus properties. Therefore, we will test whether visual stimulation introduces stimulus-specific inputs to individual neurons (or groups of neurons) in such a way that their activity can be distinguished from one another when the circuits encode visual information. Second, does changing the attributes of a visual stimulus, such as orientation, spatial frequency and contrast, change the temporal structures of V_m activity and correlation? Finally, how does the synchrony in pairs of cells at the same stage of cortical processing (complex-complex pairs) compare with pairs of cells at different stages (simple-complex cell pairs) (Gilbert, 1977; Hubel and Wiesel, 1962)?

We have found that for pairs of complex cells recorded from the superficial layers of V1 in the anesthetized cats, a range of visual stimuli could evoke high-frequency V_m fluctuations (20–80 Hz) in both cells. These high-frequency components

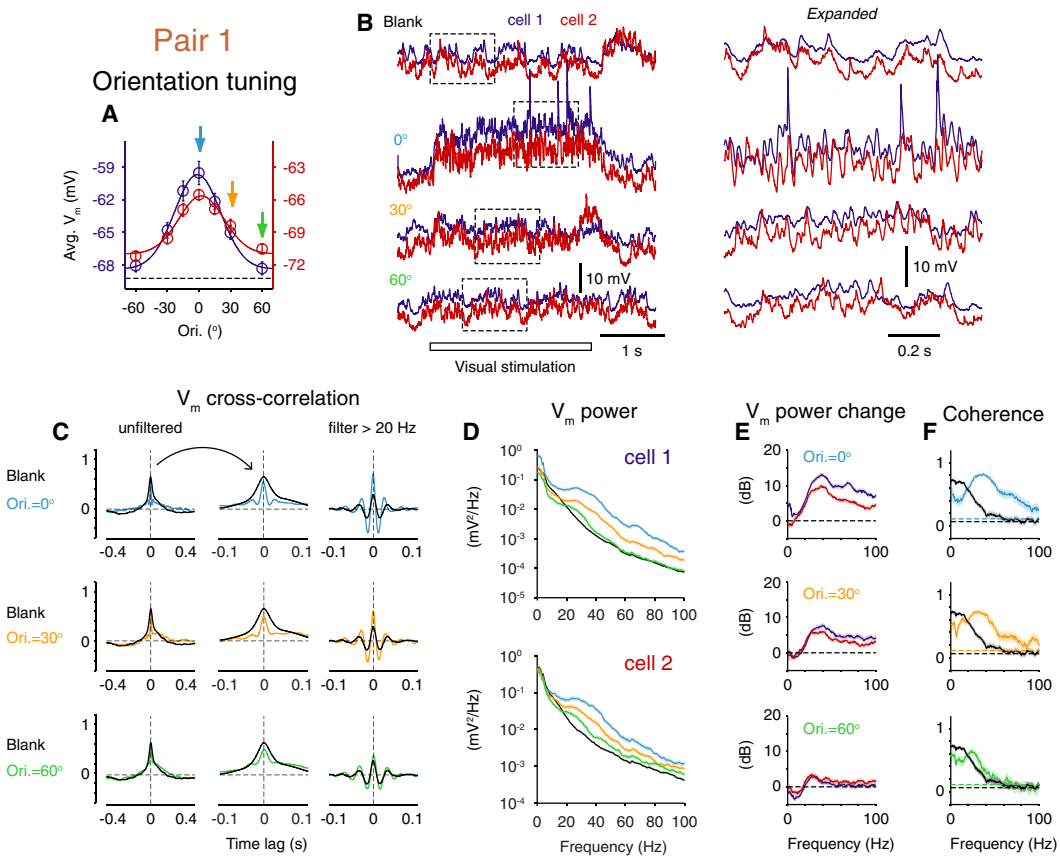

Figure 1. A Pair of Cells with Similar Orientation Preferences

(A) Orientation tuning curves of the membrane potential (V_m) of a pair of cells (blue and red) that had similar orientation preferences. Error bars show SEM. Arrows mark three representative orientation conditions (0°, 30°, and 60°) for which raw data and analysis are further illustrated. Dashed line labels the averaged V_m at rest (blank stimulus) for both cells.

(B) Example V_m records of spontaneous (blank stimulus) and visually evoked activity (0°, 30°, and 60°). Stimulation duration is indicated by the horizontal bar. Part of each trace (dashed box) is expanded to the right.

(C) V_m cross-correlations for spontaneous (black) and visually evoked (cyan, 0°; orange, 30°; green, 60°) activity (left). The central part (from −0.12 to 0.12 s) of each cross-correlation plot is expanded (middle). Cross-correlations of the high-pass filtered V_m are shown on the right.

(D) V_m power spectra for spontaneous and visual evoked activity (color codes as in C). Shaded areas are 95% confidence intervals.

(E) Spectra of the relative changes in V_m power during visual stimulation (top, 0°; middle, 30°; bottom, 60°). At each frequency, power of visually evoked activity is normalized by the spontaneous power and is expressed in decibels (dB). Shaded areas indicate 95% confidence intervals.

(F) V_m coherence spectra for spontaneous (black) and visually evoked (cyan, 0°; orange, 30°; green, 60°) activity. Dashed lines are theoretical 95% confidence limits for zero-coherence process. Shaded areas indicate 95% confidence intervals.

See also Figure S1.

were strongly synchronized between nearby complex cells regardless of whether the cells had similar or different stimulus preferences. In comparison, V_m correlation between simple and complex cells was much weaker with or without sensory input. Visual stimulation also reduced the V_m correlation at low frequencies (0–10 Hz). The spectral structure of the synchrony was only weakly dependent on the parameters of the visual stimulus and the magnitude of visual responses. Together, these data lead us to propose that in the superficial layers of V1, visual stimulation drives the circuits over several functional domains from an ongoing state with synchronized slow fluctuations into an active state with synchronized high-frequency fluctuations.

RESULTS

Neurons with Similar Orientation Preferences

We first illustrate how optimal and nonoptimal stimuli modulated V_m correlation in an example pair of neurons with nearly identical preferred orientations (Figure 1). Because the neurons in all recorded pairs were separated by no more than 500 μm, these two cells were likely located in the same orientation domain. As shown previously (Lampl et al., 1999), their spontaneous activity was strongly synchronized (Figure 1B, Blank). In the presence of a visual stimulus either at or near the preferred orientation (Figure 1B, 0° and 30°), V_m in both cells depolarized and fluctuated at high frequencies (>20 Hz). These rapid fluctuations were

strongly synchronized between the two cells, as can be readily seen at an expanded time scale. When the visual stimulus was oriented further away from the preferred orientation (Figure 1B, 60°), an increase of high-frequency fluctuations from spontaneous level became hardly visible. To quantify the correlation, we computed the V_m cross-correlations (Figure 1C, left and middle columns) and compared them for the spontaneous (black) and visually evoked (color) activity. During visual stimulation, the V_m correlation became smaller (spontaneous: 0.66; evoked: 0.55, 0.50 and 0.52 for 0°, 30°, and 60°), and narrower (spontaneous: 54 ms; visually evoked: 16, 20, and 37 ms). The narrowing corresponded to the significant increase in the synchronous high-frequency fluctuations. To isolate these components, we calculated the cross-correlations after high-pass filtering V_m at 20 Hz (Figure 1C, right column). At these frequencies, compared to the unfiltered records, visual stimulation evoked a large increase in the amplitude of the correlation (spontaneous: 0.30; visually evoked: 0.71, 0.60, and 0.40).

To study the temporal structures of the visually evoked V_m fluctuations and correlation, we applied spectral methods (Mitra and Bokil, 2008; Pesaran et al., 2002). We first obtained the power spectrum of V_m for each cell and for each stimulus condition (Figure 1D). To visualize the relative change of V_m power during visual stimulation, we plotted the ratio of V_m power during visual stimulation (relative to the spontaneous level) against frequency. Visual stimulation caused a prominent increase of power in both cells, with a maximum near 38 Hz (Figure 1E). To determine whether the visually evoked high-frequency components were correlated, we computed the coherence spectrum, which quantifies for each frequency how stably the relative phase relationship between the two signals is maintained with time. For spontaneous activity (Figure 1F, black), the coherence declined as a function of frequency (see also Poulet and Petersen, 2008). With visual stimulation (Figure 1F, color), the coherence increased and exceeded spontaneous levels at high frequencies (20–80 Hz), confirming that the high-frequency fluctuations introduced by visual stimulation were highly correlated, even more so than the spontaneous fluctuations at the same frequencies. Comparing three visual stimuli that had different levels of effectiveness in driving the cells, it is clear that the amount of synchronized high-frequency components was associated with how well the local circuits were being activated. A nonoptimal stimulus (e.g., 60°) evoked few high-frequency components. We also noticed that the temporal features and the magnitude of the visually evoked high-frequency components varied from pair to pair (two more example pairs are presented in Figure S1 available online).

Coupled with a modulation of high-frequency dynamics, optimal, and even nonoptimal, visual stimuli caused a clear decrease of coherence in the low-frequency range (0–10 Hz) (Figures 1F, compare black and color curves). This decrease of coherence was likely related to a visually induced disruption of the synchronous low-frequency V_m fluctuations during spontaneous activity (cf. Anderson et al., 2000; Finn et al., 2007; Monier et al., 2003).

Neurons with Different Orientation Preferences

When cells in a pair prefer similar stimulus orientations, the likelihood that each cell responds to any given stimulus will be tightly linked at all orientations. When cells in a pair prefer different orientations, however, whether both cells are activated or not changes with stimulus orientation. The resulting stimulus dependence of V_m synchrony in these conditions is shown for 3 pairs (pairs 4–6 in Figures 2 and S2). In the first pair (Figure 2, pair 4), two neurons differed in orientation preference by about 40° (Figure 2A). When the stimulus was oriented to activate two cells to an intermediate extent (−15°), high-frequency fluctuations were present in both cells and were well correlated (Figures 2B and 2C, −15°). When the grating was oriented to drive only one cell optimally (15°), that cell's V_m fluctuated vigorously and numerous spikes were elicited (red trace), whereas the other cell (blue trace) was only weakly activated and showed a small depolarization. Surprisingly, their V_m fluctuations were still strongly synchronized (Figures 2B and 2C, 15°). The spectra of relative power change for two cells had similar shapes in both stimulus conditions (Figure 2E, first and second plots); the coherence spectra for visually evoked activity under these stimulus conditions were quite similar (Figure 2F, first and second plots). When the visual stimulus was ineffective in driving either cell (60°), there were considerably fewer high-frequency fluctuations in both cells. Finally, common to all stimulus conditions, there was a reduction of coherence at low frequencies (Figure 2F, compare black and color curves at frequencies less than 10 Hz). Similar features can be identified in two additional example pairs shown in Figure S2 (pairs 5 and 6).

Stimulus Dependence of Membrane Potential Synchrony

The example pairs give the impression that the visually evoked change in V_m synchrony (e.g., as measured by coherence) might be weakly dependent on stimulus orientation. We analyzed this dependence in 21 pairs of cells in which visual stimulation induced strong high-frequency fluctuations. In 9 pairs, the cells had similar orientation preferences (<20° difference); in 12 pairs, the cells had different orientation preferences (≥20° difference). These two groups were analyzed separately. For comparison across pairs, in each pair, we chose one cell as a "reference" cell, and expressed the stimulus orientation relative to its preferred orientation. Additionally, we flipped the orientation order if necessary so that the preferred orientation of the second cell in the pair was always positive. The tuning curves for the 21 reference cells and corresponding second cells are shown in Figures 3A and 3B. The aggregate tuning curve for each pair is plotted in Figure 3C, where the aggregate response is represented by the normalized geometric mean response of the two cells.

To quantify the orientation dependence of synchrony, stimulus orientations were binned into four ranges (measured relative to the preferred orientation of the reference cell): −45° to −15 °, −15° to 15°, 15° to 45°, and 45° to 90°. First, we computed the averaged coherence spectrum for each stimulus orientation range and plotted them with the averaged coherence spectrum of the spontaneous activity (Figure 3D for pairs with similar orientation preferences and Figure 3F for pairs with different orientation preferences). For multiple orientation ranges, coherence at low frequencies (0–10 Hz) and at high frequencies (20–80 Hz) was modulated in opposite directions by visual stimuli,

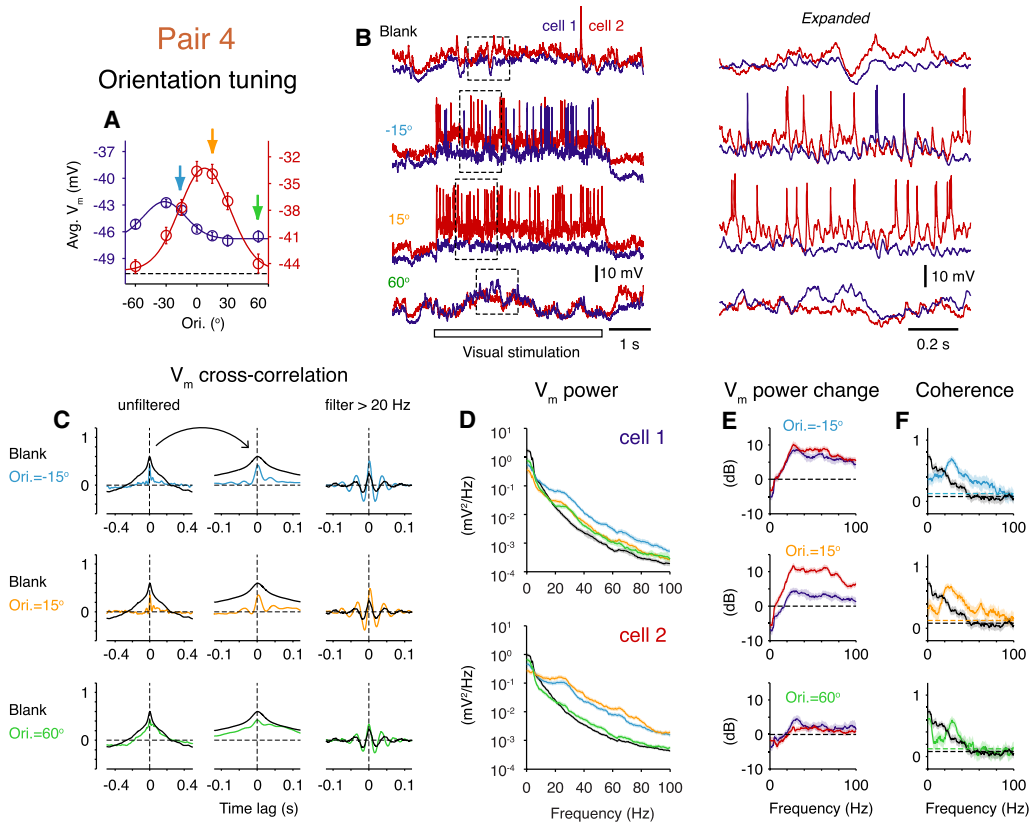

Figure 2. A Pair of Cells with Different Orientation Preferences

A pair of cells (pair 4) that had different orientation preferences. Figure layout follows the same format as in Figure 1. See also Figure S2.

consistent with previous examples (e.g., Figures 1 and 2). For any given pair, each stimulus orientation produced a corresponding change in coherence spectrum with respect to the pair's coherence in spontaneous state (e.g., Figure 1F). In each orientation range then, we estimated the mean visually evoked changes of the coherence in two frequency bands (20–80 Hz and 0–10 Hz) for the stimuli and pairs and studied their distributions (Figures 3E and 3G). For pairs with similar orientation preferences, in three ranges of stimulus orientation (from −45° to 45°), coherence during visual stimulation consistently showed a strong increase in the high-frequency band and a decrease in the low-frequency band relative to the spontaneous level (Figure 3E). For pairs with different orientation preferences, the same trend applied to an even wider orientation range, from −45° to 90° (Figure 3G). The range of orientations that evoked coherence changes either lay near the optimal orientation for one of the two cells, or between the optimal orientations of the two cells, which suggested that visually evoked changes in coherence should depend on the mean response of the pair. In Figures 3H–3K, then, we grouped the stimuli and pairs as a function of the normalized geometric mean response as shown in Figure 3C. Significant increases of coherence at high frequencies and decreases at low frequencies occurred for mean response magnitudes greater than 0.4 (Figures 3I and 3K, brown and orange). For stimuli that were ineffective in driving either cell in the pair (mean response magnitude < 0.4), the coherence rose little relative to spontaneous level at high frequencies and exhibited some decrease at low frequencies (Figures 3I and 3K, cyan).

In a limited number of pairs with prolonged recording time, we tested the effect of varying the stimulus spatial frequency or contrast on V_m correlation. Similar to what we have found for orientation dependence, synchronized high-frequency V_m fluctuations were induced by visual stimulation for conditions in which either only one cell was optimally activated or both cells were equally driven (not shown). Contrast appeared to modulate low- and high-frequency activity in a gradual manner, which suggested a competition between the pattern of spontaneous activity intrinsic to the circuits and the pattern of activity induced by sensory stimulation (Figure S3).

Dependence of Membrane Potential Synchrony on the Difference in Orientation Preferences

Example pairs and the similarity between Figures 3E and 3G indicate that visual stimulation modulates V_m synchrony regardless of whether the cells' preferred orientations are similar or not. We examined this relationship in more detail across a full set of 44 pairs (Figure 4). For this analysis, we pooled the responses if stimuli effectively activated the pair. That is, we selected stimuli for which the evoked aggregate V_m responses of the pair (the geometric mean, normalized to the maximum) were greater

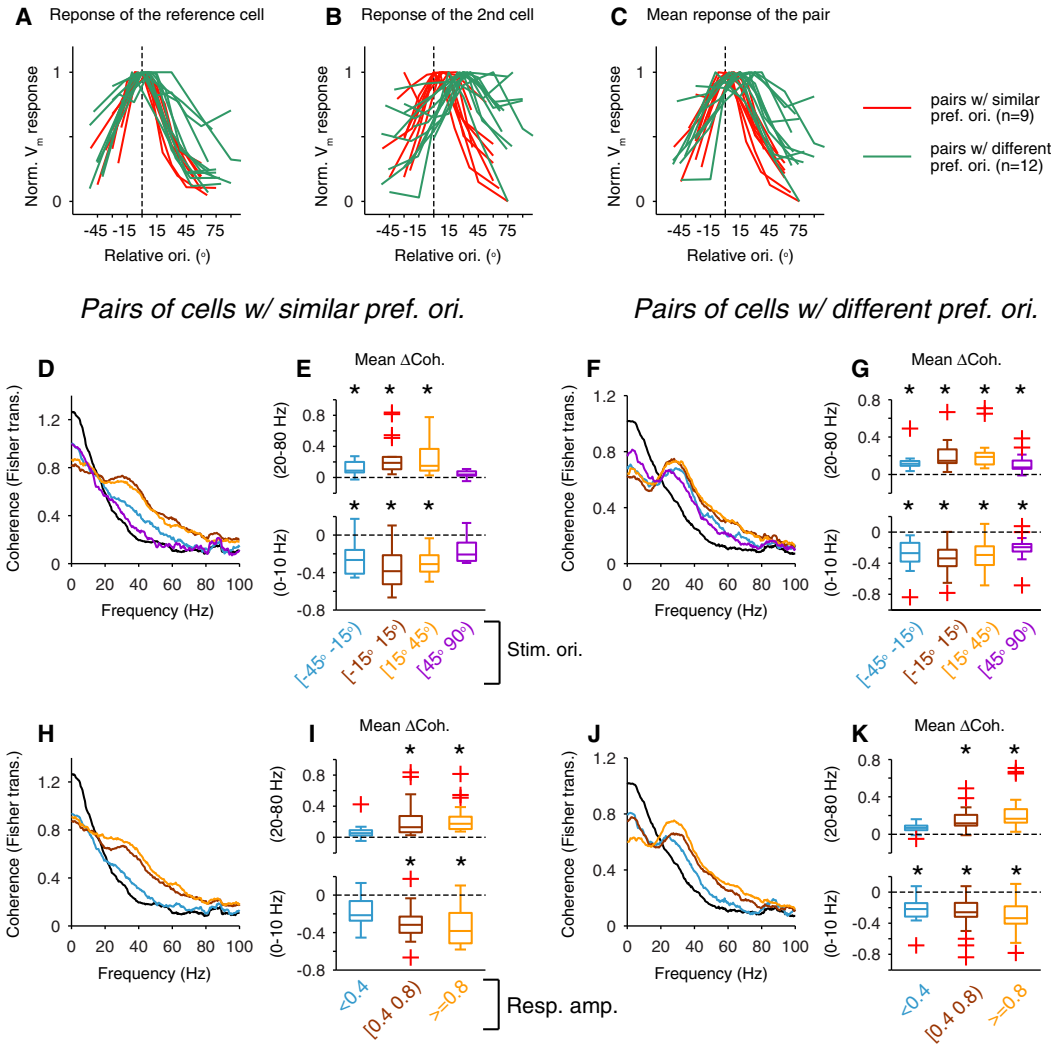

Figure 3. Stimulus Orientation Dependence of the Membrane Potential Synchrony

(A) Orientation tuning curves of the V_m response of the "reference" cell in each pair. Response amplitude is expressed as normalized DC depolarization relative to the maximal response; preferred orientations are aligned to 0. Reference cells from pairs in which two cells had similar (<20°) and different (≥20°) orientation preferences are shown in red and green.

(B) Orientation tuning curves of the V_m response (normalized DC depolarization) of the second cell in each pair. The stimulus orientations are arranged such that the preferred orientation of the second cell is positive.

(C) Orientation tuning curves of the mean response of the two cells in each pair (normalized geometrical mean of DC depolarization).

(D) Averaged coherence functions for four different ranges of stimulus orientation and spontaneous activity, for pairs with similar orientation preferences. A Fisher-transformed coherence format with bias subtracted was used for averaging (Z, see Experimental Procedures).

(E) Box-and-whisker plots show the distribution of the mean changes of coherence (relative to the spontaneous level) in the high- and low-frequency bands from samples (individual stimuli of individual pairs) within each orientation range. In each plot, central line marks the median, the box edges are the 25th and 75th percentiles and the whiskers extend to the most extreme data points that are within 1.5 interquartile range from the 25th or 75th percentiles. Data outside whiskers are outliers (red crosses). Asterisks mark significant change of coherence during visual stimulation relative to the spontaneous level (Kruskal-Wallis nonparametric test followed by a Tukey's HSD, $p < 0.05$; all data points are included for comparisons).

(F and G) Same as (D) and (E) for pairs with different orientation preferences.

(H–K) Same as (D)–(G), but the stimuli and pairs are grouped according to the mean visually evoked response of two cells (as in C), instead of stimulus orientation. See also Figure S3.

than 0.4. For example, for pairs 1 (Figure 1) and 4 (Figure 2), we pooled the responses to three orientations (−15°, 0°, and 15°); for pair 6 (Figure S2), we pooled a range between −60° and 60°.

For most pairs (42/44), effective visual stimulation reduced the V_m correlation (Figure 4A). Most of the points, whether for pairs with similar (red) or different (green) orientation preferences, lie significantly below the diagonal line (Figure 4A, open symbols). The median reduction (and interquartile range) was 20.9% (20.4%) for pairs with similar orientation preferences and 31.0% (21.5%) for pairs with different orientation

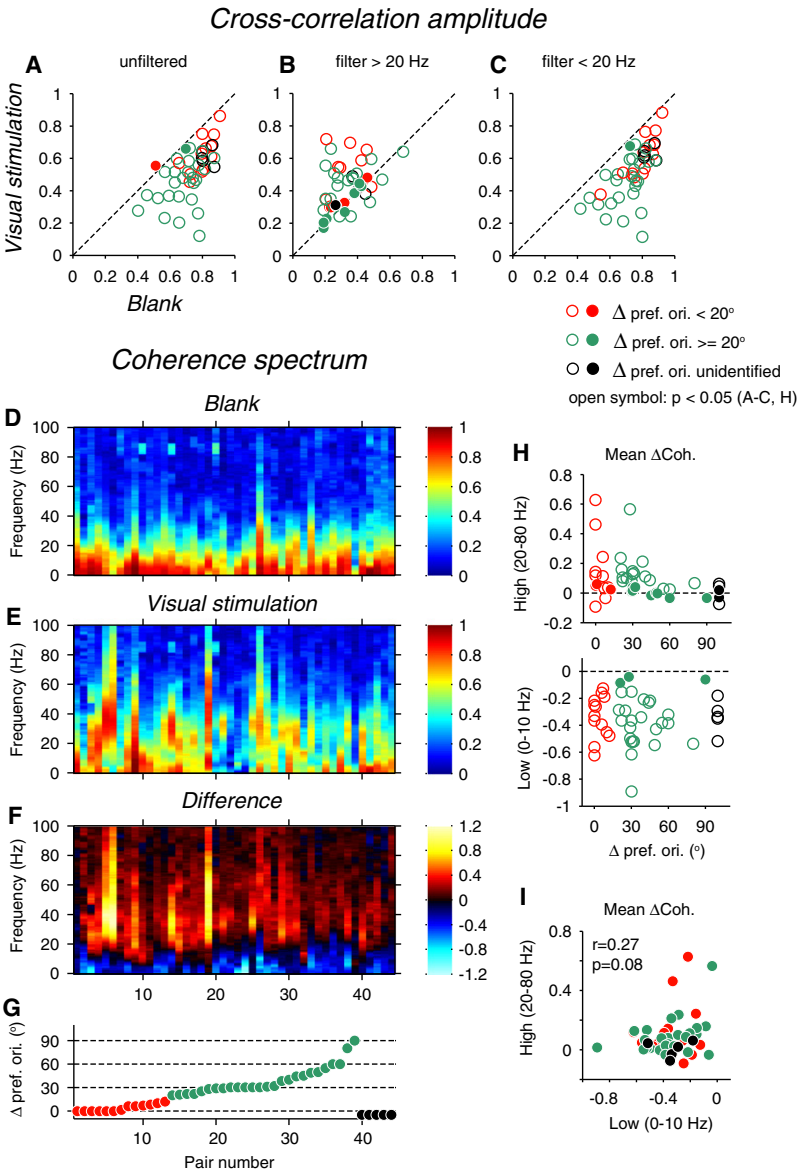

Figure 4. Summary of Correlation and Coherence Analyses for a Population of Pairs

(A) Scatter plot shows the amplitudes of the V_m cross-correlations with and without visual stimulation for each pair.

(B and C) Same as (A) with V_m high-pass filtered above 20 Hz (B), or low-pass filtered below 20 Hz (C). Points are color-coded for the relative orientation preferences of the pairs as indicated. Open symbols indicate those points that are significantly different from the identity line ($p < 0.05$, permutation test).

(D and E) Coherence of spontaneous and visually evoked activity for all pairs, expressed as colormaps. Pairs are aligned side-by-side along x axis with y axis denoting the frequency.

(F) The visually evoked change in coherence for each frequency is calculated from the Fisher-transformed coherence (Z, see Experimental Procedures). Pairs are ordered according to increasing difference in orientation preference (G).

(H) Average visually evoked change in coherence plotted as a function of the difference in orientation preference for each pair. The high- and low-frequency bands are plotted separately (above and below).

(I) Coherence changes in the high- versus low-frequency bands are not correlated across pairs.

See also Figure S4.

preferences. To distinguish the different effects of visual stimulation on low- versus high-frequency signals, we computed the cross-correlation after either high-pass or low-pass filtering V_m (Figures 4B and 4C). The reduction in Figure 4A was clearly confined to the low-frequency components (Figure 4C), whereas at high frequencies, for most pairs (37/44), visual stimulation either increased or had no effect on the correlation (Figure 4B). As expected, the width of the cross-correlation of the unfiltered V_m decreased in the presence of a visual stimulus (not shown).

To illustrate the spectral structure of V_m synchrony, we computed the coherence spectra of spontaneous and visually evoked activity for each pair and plotted the results in color maps (Figures 4D–4F). Each column represents the coherence spectrum of a distinct pair, presented in order of increasing difference in orientation preference between the cells (Figure 4G). The color maps show coherence of spontaneous activity (Figure 4D) and coherence during effective visual stimulation (Figure 4E). The difference between these two conditions (Figure 4F) was calculated from the Fisher-transformed coherence (Z; see Experimental Procedures). In Figure 4H, the change in coherence averaged over the low-frequency (0–10 Hz) or high-frequency (20–80 Hz) range is plotted against difference in preferred orientation. In Figure 4I, the average change in coherence for the high-frequency band is plotted against that for the low-frequency band.

In agreement with the results from the cross-correlation analysis in Figures 4A–4C, the overall effect of visual stimulation was to decrease the coherence at low frequencies (Figure 4F, cool colors), and increase the coherence at high frequencies (warm colors). A decrease in coherence at low frequencies occurred in most pairs (41/44), independent of orientation (Figure 4H, lower panel). An increase in coherence at high frequencies occurred primarily in pairs with difference of orientation preference between 0° and 50° (Figure 4H, upper panel). The two effects—on low- and high-frequency coherence—were not significantly correlated with each other across the population (Figure 4I). Note that the effect of visual stimulation occurred on top of the resting coherence in spontaneous activity, which was itself not dependent on the relative orientation preference (Figure 4D). Visual stimulation then either increased the high-frequency coherence, or left it largely unchanged (e.g., Figure S4) for most pairs (41/44).

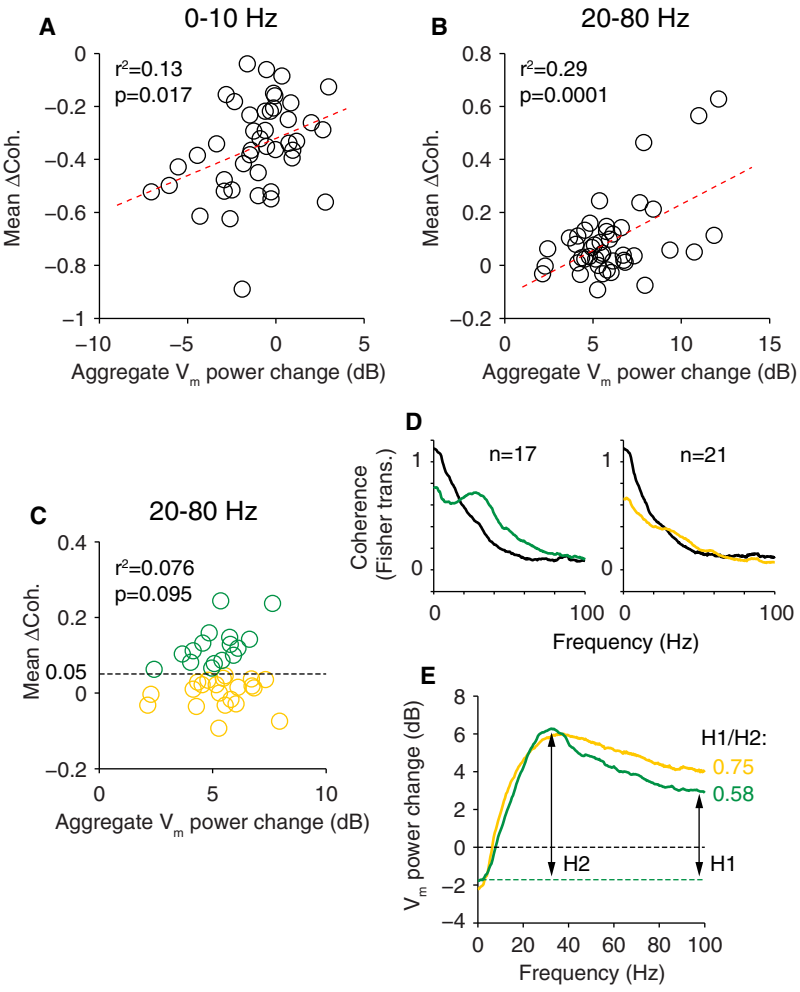

Figure 5. Relationship between Visually Evoked Changes in Membrane Potential Power and Coherence

(A and B) Average change in coherence is plotted against change in aggregate V_m power in the low-frequency (A) and high-frequency (B) bands. Each circle represents a pair. Dashed red line in each plot is the linear regression.

(C) Same as (B) but only for pairs of which the visually evoked power change at high frequencies (20–80 Hz) is less than 8 dB. Pairs are divided into two groups based on whether the mean coherence change is larger (green) or smaller (yellow) than 0.05.

(D) Coherence functions of spontaneous and visually evoked activity are averaged across pairs for two groups.

(E) Visually evoked power changes are averaged across pairs for two groups. To characterize the shape, an index (H1/H2) is calculated as illustrated.

Relationship between Visually Evoked Changes in Membrane Potential Synchrony and Power

We asked whether (and how) the visually evoked change in V_m synchrony depended on the change in V_m power. We therefore plotted the mean visually evoked change in coherence against the mean change in V_m power for low frequencies (Figure 5A) and for high frequencies (Figure 5B). Each parameter was average across frequencies (0–10 Hz and 20–80 Hz) and across the two cells of each pair. The change in V_m power (relative to the spontaneous level) was expressed in decibels. The change in coherence within the frequency band is the same as in Figure 4H.

The reduction of low-frequency synchrony was correlated with a decrease in low-frequency power (Figure 5A; r = 0.36, p = 0.017). However, the change in V_m power only accounts for 13% of the variance in change in coherence. In addition, in 25% of the cells (11/44), a decrease in low-frequency coherence was associated with an increase in low-frequency power. Therefore, visual stimulation seems to disrupt the intrinsic low-frequency, large-amplitude fluctuations in the network (e.g., up and down state transitions), and may also introduce additional low-frequency activity, thereby interfering with the low-frequency structure of the circuit dynamics. Similar phenomena may occur throughout the cerebral cortex (cf. Churchland et al., 2010).

At high frequencies (Figure 5B), the presence of visual stimulation always increased the V_m power. This increase, in turn, correlated with the increase of synchrony (r = 0.54, p = 0.0001). We noticed, however, that for a majority of pairs (38/44, 86%), the change in power was smaller than 8 dB, and for these pairs the change could not predict the change in coherence (p = 0.095; Figure 5C). To find other factors that might contribute to the change in coherence, we then separated these pairs into two groups based on whether the mean coherence change was larger or smaller than 0.05 (Figures 5C and 5D, green and yellow). Although the average power change at high frequencies was similar for these two groups of pairs (green, 5.31 dB; yellow, 5.35 dB; p = 0.92, permutation test), the shapes of the spectrum of relative power change were different in that pairs with larger coherence increase had sharper peaks, centered near 33 Hz (Figure 5E). We calculated an index that captured how peaked the spectrum curve was—the power change at 100 Hz divided by the that at the peak, each measured with respect to the power change between 0 and 2 Hz (Figure 5E, H1/H2). Pairs with larger coherence increases had smaller indices, meaning that their relative power spectra were on average more peaked (0.58 versus 0.75, p = 0.005, permutation test).

Contribution of Membrane Potential Synchrony to Spike-Triggered Average of Membrane Potential

In previous studies using paired intracellular recordings, strong V_m synchrony caused the spike-triggered V_m average (V_m STA) between neurons to straddle the spike time (cf. Gentet et al., 2010; Lampl et al., 1999; Poulet and Petersen, 2008). This "average synchronous excitation potential," or ASEP, was initially identified in combined intracellular-extracellular recordings from monkey motor cortex by Matsumura et al. (1996) and is distinct from the V_m STA caused by monosynaptic

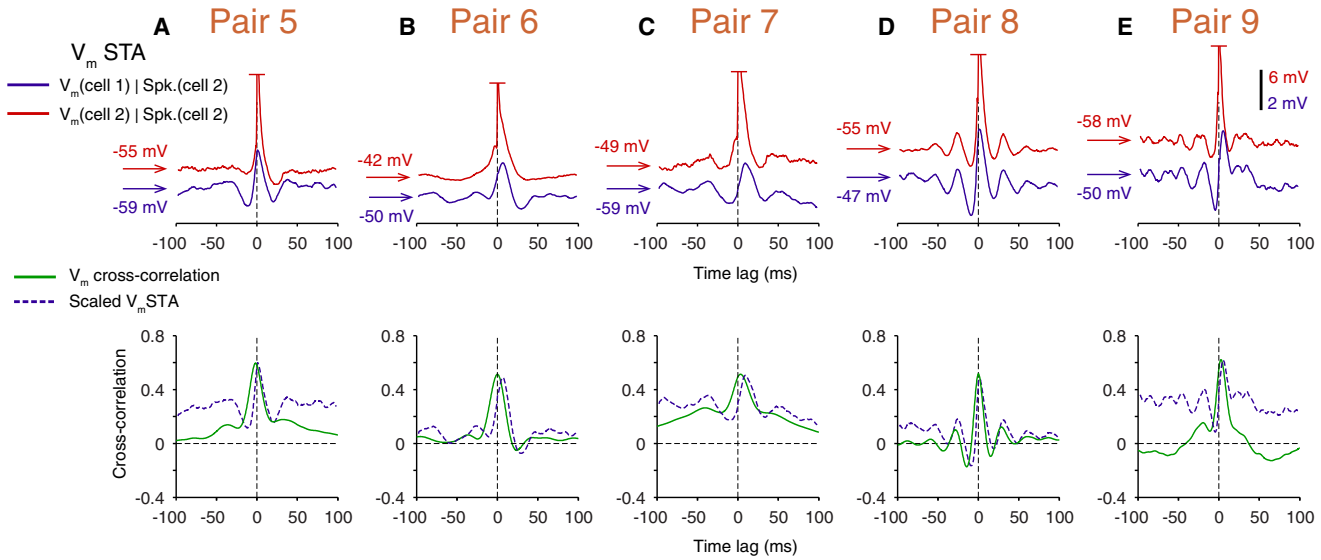

Figure 6. Correlation of Spike and Membrane Potential between Pairs of Cells

(A–E) Spike-triggered averages of V_m (V_m STAs) from intracellularly recorded pairs of cells. Top row, blue traces (cross-neuron V_m STAs) are the STAs of cell 1's V_m using cell 2's spikes as triggers and the overlying red traces (intrinsic V_m STAs) are the STAs of cell 2's V_m triggered by its own spikes. Bottom row, V_m cross-correlations for the same pairs (green). Dashed blue lines are manually scaled cross-neuron V_m STAs. All data are from visually evoked activity.
See also Figure S5.

connections (cf. Bruno and Sakmann, 2006). Can V_m synchrony during visual stimulation also lead to an ASEP-like V_m STA? To test this possibility, we constructed V_m STA for seven intracellularly recorded pairs of cells, five of which are illustrated in Figure 6. For each pair, the trigger cell was marked as cell 2. Its spike times were used to average its own V_m (red, intrinsic V_m STA) or V_m of the other cell in the pair (cell 1, blue, cross-neuron V_m STA). Note that these V_m STAs were derived from unfiltered visually evoked activity; during spontaneous activity too few spikes were available for computing reliable V_m STAs (for an example that compares spontaneous and evoked cross-neuron V_m STAs, see Figure S5). In all pairs, the onset of the cross-neuron V_m STAs preceded the spike time, arguing against the possibility that these V_m STAs were caused by a direct monosynaptic input from the trigger cell, which should instead have an onset after trigger time, a rapid rising phase and a slow decay phase (Bruno and Sakmann, 2006). In every pair, the shape of the cross-neuron V_m STA resembled that of the intrinsic V_m STA, albeit with smaller amplitude, indicating that the fast V_m fluctuations are responsible for eliciting spikes and are correlated between neurons (Figures 6A–6E, compare blue to red traces). For each pair, we also scaled the cross-neuron V_m STA and compared its shape with the shape of V_m cross-correlation (Figures 6A–6E, bottom). The shape of cross-neuron V_m STA was similar to the shape of V_m cross-correlation with a small narrowing and small offsets in the rising phase and peak time, which would be expected given that spikes are preferentially elicited during the rising phase of the response. These observations are consistent with the proposal that V_m synchrony can lead to a V_m STA similar to ASEP (for a similar finding on local field potential, see Okun et al., 2010).

Simple-Complex Cell Pairs

So far we have focused on describing pairs of complex cells recorded from the superficial layers of V1 (200–600 μm depth). We also asked whether V_m synchrony exists across different cortical layers, in particular, between layer 4 (and deep layer 3), where thalamic afferents terminate and simple cells dominate, and layer 2/3, which is considered to be a subsequent stage of cortical processing and mostly contains complex cells that do not receive direct geniculate inputs (Alonso and Martinez, 1998; Gilbert, 1977). We recorded six pairs that each contained one simple and one complex cell. One pair (pair 10), in which the two cells had the same orientation preference, is illustrated in Figures 7A–7F. The orientation tuning for the simple cell was derived from the F1 component of V_m, and for the complex cell from the mean V_m, or DC component (Figure 7A). Since the electrode tips were close to one another in the horizontal direction, the cells were probably located in the same orientation column but in different layers. Compared to the complex cell pairs seen earlier, this pair showed much lower V_m correlation in the absence of stimulation (Figure 7B, first row). The membrane potential of the simple cells was never quiet, whereas the complex cell's potential became nearly flat between the large depolarizing events. The large-amplitude depolarizing bumps that occurred at low frequencies in the complex cell had roughly comparable counterparts in the simple cell, but the match between the two waveforms was much less precise than in the complex cell pairs (for example, Figure 1). Overall, the spontaneous activity of two cells had a low correlation (0.4; Figure 7C, left and middle column, black trace), smaller than almost all of the complex cell pairs (Figure 4A). Most of this correlation was due to activity below 20 Hz, since high-pass filtering with a cutoff

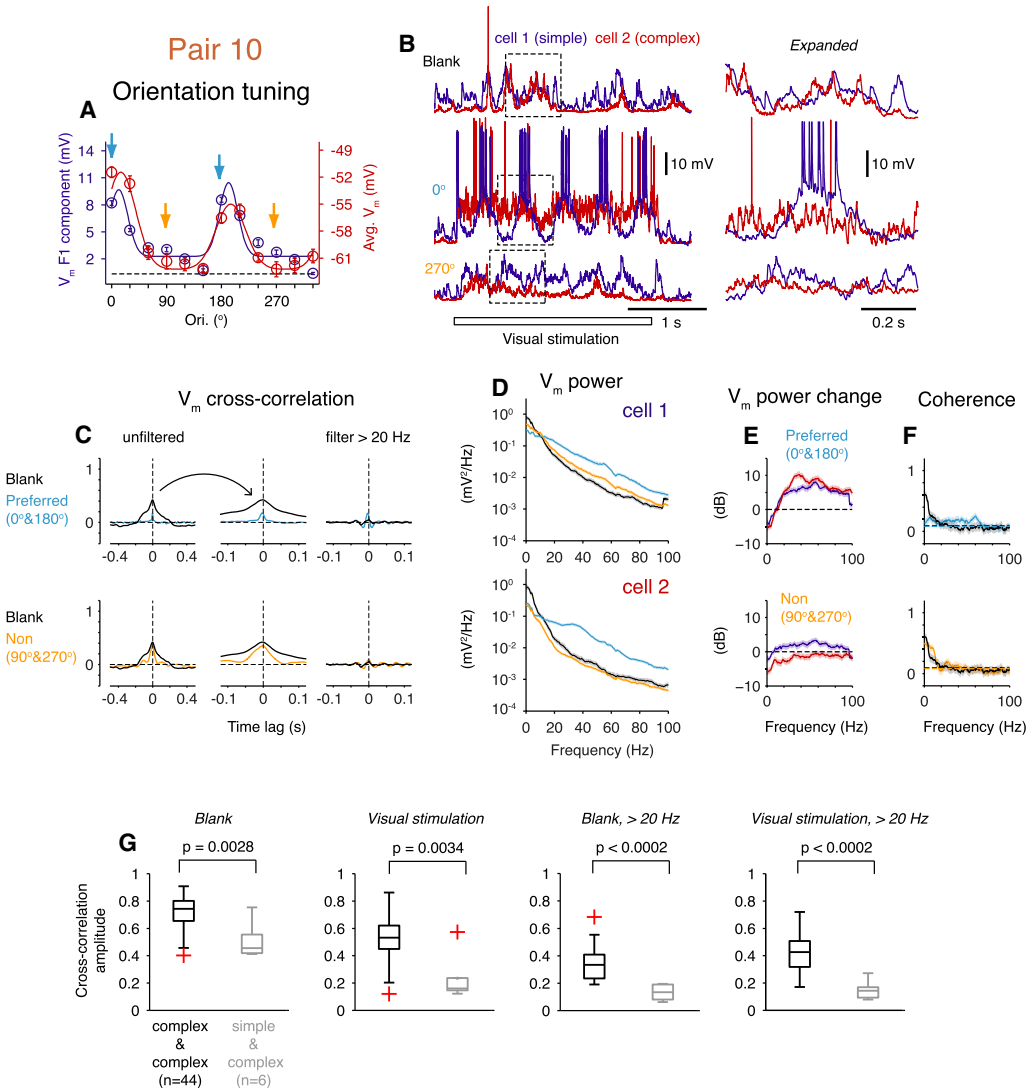

Figure 7. Weak Membrane Potential Correlation between Simple and Complex Cells

(A–F) A pair composed of a simple cell (blue) and a complex cell (red) that had matched orientation preferences. Raw data and analysis from spontaneous activity (black), preferred stimulation (cyan, 0° and 180°) and nonpreferred stimulation (orange, 90° and 270°) are illustrated. Figure organization follows the format as in Figure 1.

(G) Comparison of the V_m cross-correlation amplitudes between pairs that contained two complex cells and pairs that contained one simple cell and one complex cell. Cross-correlations were calculated for spontaneous and visually evoked records with and without high-pass filtering the V_m. Statistical differences were verified by Kruskal-Wallis nonparametric test.

See also Figure S6.

of 20 Hz removed much of the correlation (Figure 7C, right column, black trace). This result is also reflected in the coherence spectrum for spontaneous activity (Figure 7F, black trace), which shows significant coherence only at frequencies below 20 Hz.

We can now ask how V_m synchrony responds to the presentation of optimal visual stimulation. During optimal stimulation, spiking activity is largely confined to the column containing these cells. It might be, then, that the cells' V_m becomes much more correlated. This is not the case, however. Membrane potential responses to preferred (0°) stimulation are shown in Figure 7B (second row). By the definition of simple and complex cells, the temporal patterns of visually evoked responses in the two cells were very different, the simple cell showing strong modulation of both V_m and spike rate at the stimulus frequency (2 Hz), in contrast to the complex cell which gave an unmodulated response. As in the complex cell pairs, optimal stimulation caused a decrease in the amplitude and width of the correlation (Figure 7C, first row, left; note that the stimulus component of the evoked response was removed before cross-correlation was calculated). The overall reduction might correspond to a strong decrease in the correlation of the low-frequency components

and a weak increase in the correlation of the high-frequency components (Figure 7C, first row, right). During visual stimulation, high-frequency components of the complex cell only had a weak correlation with those in the simple cell and the coherence was about one-third of those seen in complex-complex pairs (Figure 7F, compare the coherence value of 0.18 at 20–40 Hz with the coherence of previous complex cell pairs in similar frequency range). Visual stimulation increased the high-frequency V_m power in the simple cell without a distinctive peak in either the V_m power spectrum (Figure 7D, cyan) or the spectrum of relative power change (Figure 7E, top), in contrast to the complex cell. Nonpreferred stimulation (e.g., 270°; Figure 7B, third row) also narrowed the width of the correlation but left the amplitude nearly unchanged (Figure 7C, second row).

Two more simple-complex pairs are shown in the Figure S6 (pairs 11 and 12). In these pairs, V_m fluctuations of the simple cells lagged behind those of the complex cells during spontaneous activity and most of the correlation was again caused by low-frequency activity. Although visual stimulation evoked an increase in high-frequency power in both simple and complex cells, it did not cause a strong increase in synchrony. Finally, comparing the distribution of correlation amplitudes between complex-complex pairs and simple-complex pairs for spontaneous and visually evoked activity confirmed the lack of strong V_m correlation for paired simple and complex cells (Figure 7G).

Previous literature has suggested that simple cells might be a relatively heterogeneous group. For example, some simple cells may derive most of their excitatory input from the lateral geniculate nucleus (LGN), whereas some receive most of their input from other cortical cells (Finn et al., 2007). It then seems likely that simple cells become engaged with the complex cell circuits to different degrees. Some simple cells from previous reports, for example, have more high-frequency fluctuations than the ones analyzed here (e.g., Cardin et al., 2005, 2007; Gray and McCormick, 1996), although it is still not known to what degree that these fluctuations were synchronized with those in complex cells.

DISCUSSION

By recording membrane potential (V_m) from pairs of V1 neurons in vivo, we have studied how visual stimulation modulates the correlation of V_m fluctuations between nearby cells. First, high-frequency V_m fluctuations induced by visual stimulation were strongly synchronized. Not only was the synchrony observed between neurons that belonged to the same functional domain, in addition, there was strong synchrony between neurons lying in different functional domains (e.g., Figures 1 and 2). Second, visual stimulation changed the spectral structure of the V_m correlation that was present in the spontaneous state, suppressing coherence at low frequencies (0–10 Hz) and maintaining or facilitating coherence at high frequencies (20–80 Hz; Figures 1–4). Third, for a pair of cells, a broad range of stimuli caused comparable effects on V_m synchrony (Figure 3). Fourth, during visual stimulation, V_m synchrony gave rise to a synchronous form of cross-neuron V_m STA that has an onset preceding the trigger time (Figure 6). Last, in contrast to pairs of complex cells, the high-frequency fluctuations were only weakly synchronized between simple and complex cells (Figure 7). These findings extend the former work (Lampl et al., 1999) by revealing the dependence of V_m synchrony on the stimulus properties, the cells' stimulus specificity, and the relationship between them.

Relationship with Previous Studies

Many intracellular studies in V1 have found that sensory stimulation evokes high-frequency V_m fluctuations (e.g., Anderson et al., 2000; Azouz and Gray, 2008; Bringuier et al., 1997; Cardin et al., 2005, 2007; Douglas et al., 1991; Gray and McCormick, 1996; Jagadeesh et al., 1992; Priebe et al., 2004; Volgushev et al., 2003). In studies where the temporal features of the high-frequency activity were analyzed, some focused on the membrane potential correlate of gamma-band dynamics as identified in LFP and spike records (Cardin et al., 2005; Gray and McCormick, 1996; Jagadeesh et al., 1992; Volgushev et al., 2003), whereas others found far less power in the gamma band and instead reported selective fluctuations in the lower frequency band, for instance, 7–20 Hz (Bringuier et al., 1997). In our work, we encountered a variety of temporal patterns for visually evoked changes in V_m power: the majority were still in the beta-gamma range (20–80 Hz, often centered around 30–40 Hz), but occasionally we did record relatively slower fluctuations (<20 Hz, not shown).

Regardless of where in the spectrum the evoked V_m fluctuations predominated, they were synchronized between pairs of neurons and were often more synchronized than the spontaneous activity in the same frequency range. Therefore, high-frequency V_m fluctuations observed in single neurons often represent a large-scale coherent activity in the local network, rather than being unique for individual cells. It is worthwhile to mention that the power spectrum of V_m itself always has an overall 1/f structure. When superimposed on the 1/f background, the distinctive peak of the V_m power during visual stimulation appears as a small convexity in the overall spectrum (e.g., Figures 1D and 2D). Therefore, the spectrum of relative power change induced by visual stimulation better illustrates the spectral features of the visual response (Figure 5E; cf. Berens et al., 2008a; Henrie and Shapley, 2005).

A number of studies have examined the correlation of spike times between pairs of V1 neurons and found precisely correlated firing, that is, spike cross-correlograms straddling zero time lags, with widths on the order of ten milliseconds or less (Das and Gilbert, 1999; Jermakowicz et al., 2009; Kohn and Smith, 2005; Maldonado et al., 2000; Smith and Kohn, 2008; Toyama et al., 1981a, b; Ts'o et al., 1986). These cross-correlograms are reminiscent of the narrowed V_m cross-correlations during visual stimulation that we observed and can occur for activity of neurons belonging to the same or different orientation domains. This type of spike cross-correlograms is usually interpreted as an indicator of common inputs (Perkel et al., 1967). However, in the cortical circuits, due to the complex synaptic connections, the identity, the number of the common inputs, or their strength relative to the total synaptic inputs cannot be determined from spike correlations (cf. de la Rocha et al., 2007). Moreover, the existence of common inputs to nearby cells is still debatable (Ecker et al., 2010). With dual whole-cell recordings, we directly examined the subthreshold V_m correlation

between nearby neurons during visual stimulation. For pairs of neurons, V_m fluctuations were continuously synchronized at high frequencies. It is therefore to be expected that, once the depolarizing transients exceeded thresholds of both cells, they would fire synchronous spikes. Even in the absence of synchronous spikes however, the two cells' synaptic inputs were still highly synchronized during the entire stimulation period. Therefore, as Lampl et al. (1999) have alluded to, this finding rules out an alternative mechanism, that the precisely correlated firing between pairs of V1 neurons is caused by brief and sporadic synchronized events that add to a constant barrage of uncorrelated inputs. Since V_m synchrony exists for neurons with different functional properties and for responses to a wide range of visual stimuli, common inputs, namely, shared axonal innervations, may not be required for intracortical spike synchrony (cf. Usrey and Reid, 1999).

Compared to V_m synchrony, the strength of spike synchrony is small in most reports (0.001–0.01 coincidence per spike in Kohn and Smith, 2005; Smith and Kohn, 2008). This difference could be explained by a number of factors: difference in the excitability of two neurons, difference in the amplitudes of high-frequency fluctuations, or less-correlated slow V_m fluctuations during visual stimulation, which sometimes slowly and asynchronously modulate the distance between the baseline V_m and threshold.

V_m synchrony of neuronal pairs gives a different picture of the stimulus dependence than spike synchrony does. Kohn and Smith (2005) reported that spike synchrony was strong when both cells were driven well by a stimulus and declined quickly as stimulus orientation became ineffective. In our data, however, increase in high-frequency coherence (and the decrease in low-frequency coherence) could be induced over a wide range of stimulus orientations (Figure 3). This range includes stimuli that drive both cells well (spikes or subthreshold depolarization), those that drive only one cell but are suboptimal in the other cell, and those that drive both cells suboptimally. With intracellular recording, then, it is possible to detect changes in input correlation for conditions under which spike synchrony cannot be measured. In other words, spike threshold masks much of the subthreshold synchrony that contains critical information about synaptic inputs that the circuits are producing (Carandini, 2004; Priebe and Ferster, 2008; Priebe et al., 2004). A reduction in the spike cross-correlogram height, therefore, does not necessarily indicate a commensurate reduction in common inputs (e.g., Figure 11 in Ts'o et al., 1986).

In the primary visual cortex, visual stimulation induces gamma-band (25–90 Hz) power increases in the LFP (Berens et al., 2008b; Gray and Singer, 1989; Henrie and Shapley, 2005; Siegel and König, 2003). Additionally, as quantified by spike-field coherence analysis and spike-triggered field averages, spike times of individual V1 neurons, and in particular multiunit activity, are temporally correlated with the LFP fluctuations in the gamma-band, which suggests synchronous ensemble activity in the local network (Engel et al., 1990; Gray et al., 1989; Gray and Singer, 1989; Henrie and Shapley, 2005; Siegel and König, 2003). The synchrony of high-frequency V_m fluctuations that we have observed in cell pairs likely contributes to these observations.

From our own and previous results, it is tempting to suggest that V_m synchrony is a fundamental rule that governs the activity in the primary visual cortex (see also Matsumura et al., 1996). By establishing V_m synchrony within the same functional domain and across different functional domains, neurons could potentially coordinate their activity with each other, instead of behaving independently. For example, multiple neurons can fire precisely correlated spikes that should have a synergistic impact on postsynaptic targets (Tiesinga et al., 2008). On the other hand, the V_m fluctuations of weakly driven cells during nonoptimal stimulation can synchronize with those of well-driven cells (e.g., Figure 2). Thus, lateral interaction between different functional domains may not need to rely on purely excitatory or inhibitory mechanisms."

Neuronal Circuits for Synchronous Activity

Our results raise two questions concerning the underlying neuronal circuits that produce the synchronous V_m fluctuations. First, what are the synaptic conductance components underlying the ever-changing V_m fluctuations (Brette et al., 2008; Okun and Lampl, 2008)? In neocortical and hippocampal circuits, coactivation and instantaneous correlation between synaptic excitation and inhibition are critical for producing slow or fast V_m fluctuations (Atallah and Scanziani, 2009; Haider et al., 2006; Okun and Lampl, 2008), which may also be responsible for generating V_m fluctuations that we have seen in spontaneous and visually evoked activity in V1 cells. In addition, inhibitory circuits may play a role in orchestrating the synchronization of the local circuits (Cardin et al., 2009; Hasenstaub et al., 2005). Second, what components of the circuit architecture are required for synchrony? Visual stimuli predominately increase the activity of a pool of superficial layer neurons that represent its features. These well-driven neurons, however, could make widespread horizontal connections in the same layers and send out their activity, for example, in the form of high-frequency fluctuating inputs, to other neurons that are not driven to fire strongly. Therefore, we hypothesize that the mechanism of V_m synchrony could likely be rooted in the recurrent network in superficial layers. Specifically, the axonal and dendritic arbors of V1 neurons in superficial layers are locally nonspecific and dense, as opposed to selective targeting of distant domains with similar preferences (Binzegger et al., 2004; Bosking et al., 1997; Gilbert and Wiesel, 1989). Such cortical architecture, which was thought to produce synchronous spiking between nearby neurons that had similar or different functional properties (cf. Das and Gilbert, 1999; Kohn and Smith, 2005; Ts'o et al., 1986), could be responsible for establishing V_m synchrony. Indeed, the role of axonal arbors in propagating synchronous fluctuations has been proved with optogenetic methods in rodent barrel cortex (Adesnik and Scanziani, 2010).

What causes the high-frequency components during visual stimulation and why do they often become more coherent than spontaneous fluctuations in the same frequency band? A number of factors might contribute. For evoked activity, the excitatory synaptic drive to superficial layer neurons mainly comes from feed-forward inputs originating in the thalamo-recipient layers and the recurrent excitation in the same layers and is more or less concentrated, but is not confined (Bringuier

et al., 1999), to the part of cortex that represents the visual field that is being activated. This distinguishes evoked activity from spontaneous activity, which might originate from different sources (Sakata and Harris, 2009). Therefore, the fast and synchronous activity may be inherent in the response transformation from simple to complex cells and may therefore depend on specific action on excitatory and inhibitory neurons or the recruitment (or suppression, see for example Niell and Stryker, 2010) of a different portion of the inhibitory network.

The Anesthetized versus the Awake Brain

We made dual-whole cell recordings in anesthetized animals using two different anesthetics (Experimental Procedures). Does comparable V_m synchrony exist in the awake cortex? Poulet and Petersen (2008) have observed highly correlated V_m fluctuations in awake mouse during quiescent states. The overall correlation decreases (by more than 50%) when the animal starts to behave (whisking). Recently, the same group extended their findings to inhibitory circuits (Gentet et al., 2010). Similarly, Okun et al. (2010) have found strong correlation between V_m and LFP signals that matches the spike-triggered field average in the cortex of awake rats. The magnitude of this correlation is also related to the rat's behavior (e.g., quiet versus moving) and the corresponding brain states. These results seem to indicate that V_m synchrony in awake animals decreases dramatically when the animal is engaged in certain behaviors. However, such modulation is largely restricted to the low-frequency ongoing activity in the quiet, awake animals, similar to the effect of visual stimulation on the V1 circuits (e.g., our results; see also Kohn and Smith, 2005; Nauhaus et al., 2009). It is not yet clear whether the modulation of high-frequency membrane potential synchrony that we described occurs in awake, behaving animals.

Extracellular recordings of spikes and field potentials also suggest that synchronous activity in cortical circuits is not confined to the anesthetized brain. By criteria such as spike-field coherence, spike-triggered field average, and spike time correlation, synchronous activity in neocortical (including the primary visual cortex) and subcortical structures has been reported in numerous studies of awake behaving animals (for review, see Fries, 2009). The synchronization can be induced passively by visual stimulation (e.g., Ray and Maunsell, 2010; Siegel and König, 2003; Vinck et al., 2010), and can also be modulated by cognitive functions, such as attention (Fries et al., 2001) and memory (Pesaran et al., 2002). It remains to be investigated whether extracellular findings on synchronization could be accounted for by V_m synchrony among a large population of local neurons. An intriguing possibility is that V_m synchrony not only exists but is even more versatile in the awake brain and is fundamental to many cognitive functions, including perception.

EXPERIMENTAL PROCEDURES

Animal Preparation

Anesthesia was induced in adult female cats aged 4–6 months with ketamine hydrochloride (30 mg/kg i.m.) and acepromazine maleate (0.3 mg/kg i.m.), and was maintained by intravenous infusion of sodium thiopental (20 mg/kg initial; 1–2 mg/kg/hr maintenance) or a mixture of propofol and sufentanil (5–10 mg/kg/hr + 0.75–1.5 μg/kg/hr, i.v.). After initial surgery, paralytic (vecuronium bromide, 1.5 mg/kg initial dose, 0.2 mg/kg/hr maintaining rate) was administered and the animal was artificially ventilated through a tracheal cannula (end-tidal CO_2: 3.6%–4.0%). To improve recording stability, the thoracic vertebrae were suspended and a bilateral pneumothoracotomy was performed. Body temperature was feedback controlled with a heating lamp at 38°C. Depth of the anesthesia was assessed by EEG pattern and heart rate stability. All vital parameters (heart rate, EEG, CO_2 ratio, and temperature) were continuously monitored and recorded. All procedures were approved by the Northwestern University Animal Care and Use Committee.

Visual Stimulation

The pupils were dilated with 1% atropine and the nictitating membranes retracted with 2.5% phenylephrine hydrochloride. Contact lenses were inserted and corrective lenses were placed to focus the retina on a computer monitor (ViewSonic, Walnut, CA) 50 cm distant from the eyes. Sinusoid drifting gratings were generated on the monitor using the Psychophysics toolbox (Brainard, 1997; Pelli, 1997) running under Matlab (MathWorks, Natick, MA). The monitor refresh rate and mean luminance were 100 Hz and 20 cd/m^2.

Gratings were usually less than 4 degrees in radius and were large enough to cover the receptive fields of both cells in a recorded pair. Stimuli were presented monocularly, although binocular stimulation did not change the basic findings on V_m synchrony. For studying orientation dependence of synchrony, the stimulus spatial frequency was chosen to lie between the optimal spatial frequencies of two cells in a pair. In each trial, a blank period (0.25–1 s) preceded and followed visual stimulation (1.5–4 s). One or two blocks of blank stimulation were presented for each set of stimuli. Stimuli in a set were presented in random order and the set was repetitively presented for 5–20 times.

Electrophysiology

Whole-cell recordings (Ferster and Jagadeesh, 1992) were obtained with glass electrodes filled with the internal solution that contained (in mM): 135 K-gluconate, 4 KCl, 10 HPEPS, 0.5 EGTA, 10 Na_2-phosphocreatine, 4 Mg-ATP, and 0.4 Na_2-GTP (pH 7.3, 292 mOsm). The electrode resistance ranged from 7 to 12 MΩ. Electrodes were introduced through a craniotomy, usually 2 mm wide and 6 mm long, at Horsley-Clarke posterior 1–7 mm and near the midline. The electrodes were placed 500–700 μm apart at the cortical surface, angled at 25° relative to one another so that their tips approached each other as they were driven into the brain. Warm agar solution (3% in saline) was applied to cortical surface to reduce brain movement. Cell pairs were included in the analysis only if the resting V_m of each cell was stable and was more hyperpolarized than −45 mV for long enough (15–60 min) so that we could record data from multiple sets of stimulus presentation. V_m was recorded using an Axoclamp 2A amplifier in bridge mode, anti-alias filtered and sampled at 20 kHz. To reduce capacitive coupling between the two electrodes, a grounded metal plate was inserted between them. In some experiments (Figure S5), one recording from a pair was left in juxtacellular mode.

Data Analysis and Statistics

For each pair, nonoverlapping blocks (1 s in length) of the spontaneous data were prepared for cross-correlation and spectral analysis through a few steps: (1) spike removal by interpolating the beginning and the end of spikes (Bruno and Sakmann, 2006), (2) subtraction of the DC component so that each block had zero mean, (3) resampling the data from 20 kHz to 4096 Hz, (4) removal of line noise (60 Hz and its harmonics) using Chronux routines (http://chronux.org), and (5) smoothing by Savitzky-Golay filtering (Matlab *sgolayfilt* function). For visually evoked data, we used only the first 1 or 2 s of the responses (0.25–2.25 s after stimulus onset or 0.25–1.25 s if the stimulation duration was less than 2.25 s). In addition to the steps listed above for spontaneous data, for each stimulus condition, we also subtracted the stimulus-averaged V_m response in order to remove stimulus-locked component. This step was not critical for complex cells, since by definition they show little temporal modulation at the stimulus frequency (or higher harmonics).

After the above preparation, cross-correlation of V_{m1} and V_{m2} for each block of data was calculated as follows (Matlab *xcorr* function):

$$R_{12}(\tau) = \frac{\sum_{t=1}^{N-\tau} V_{m1}(t+\tau)V_{m2}(t)}{\sqrt{\sum_{t=1}^{N} V_{m1}^2(t) \sum_{t=1}^{N} V_{m2}^2(t)}}, \tau \geq 0;\ R_{12}(\tau) = R_{21}(-\tau), \tau < 0$$

where N is the total number of data points (4096 for 1 s block) and τ is the time lag. Cross-correlations of all blocks were then averaged for each stimulus condition. The peak of the cross-correlation was taken as the maximum within 10 ms of zero time lag; the full width of the correlation was measured at half height. Since subtraction of mean response eliminated most stimulus-locked components, the cross-correlation for shift-predictor data (shifted by one trial) was flat (not shown), with no significant peaks near zero time lag. We therefore did not subtract the cross-correlation of shift-predictor from that of normal cross-correlation data. To estimate the significance of visually induced changes in correlation (Figures 4A–4C), we used a Monte-Carlo permutation test (10,000 times). Cross-correlation functions were also estimated for data that were high-pass filtered (20 Hz Butterworth).

Power spectrum and coherence were computed using multitaper methods (Mitra and Bokil, 2008) with the open-source Chronux routines (http://chronux.org/). For all spectral estimates, we applied 7 Slepian data tapers on 1 s data blocks. To assess the effect of visual stimulation on V_m power, we normalized the V_m power during visual stimulation to that in the spontaneous state and expressed the normalized power in dB: $10\log_{10}(S_{evoked}(f)/S_{blank}(f))$. The cross-spectrum of two signals was normalized by the auto-spectra of individual signals to give an estimate of coherency, $C(f)$, whose amplitude, termed coherence ($|C(f)|$), ranges from 0 to 1. The 95% confidence limit was estimated theoretically for a process with zero coherence and displayed in all coherence spectra as a dashed line (Mitra and Bokil, 2008). We also calculated 95% confidence intervals for power and coherence estimates using a jackknife procedure and plotted them as a shaded area surrounding the average. In example pairs, the 95% confidence intervals can be readily used to assess whether the visually evoked change of coherence is significant: nonoverlapping confidence intervals necessarily indicate that the difference is significant ($p < 0.05$, note however that the converse is not true). We have also confirmed the statistical significance using the method presented in (Bokil et al., 2007) but did not show the results of this method in order to reduce the data density in figures. In some other analyses, to study the mean change of coherence over a frequency range (e.g., 20–80 Hz) and examine the visually induced effect over different pairs (Figures 3D–3K, 4F, 4H, 4I, and 5), we applied a Fisher transformation for variance stabilization and then subtracted a sampling bias term as follows:

$$Z(f) = \tanh^{-1}(|C(f)|) - \frac{1}{2M-2},\ M = N_b \times 7$$

where N_b is the number of data blocks, 7 is the taper number and 2M is the degrees of freedom (Bokil et al., 2007; Mitra and Bokil, 2008). For these analyses, visually evoked change of coherence was calculated and statistical tests (e.g., permutation test; Maris et al., 2007) were performed on Z.

SUPPLEMENTAL INFORMATION

Supplemental information for this article includes six figures and can be found with this article online at doi:10.1016/j.neuron.2010.11.027.

ACKNOWLEDGMENTS

We thank Drs. Ilan Lampl, Nicholas J. Priebe, and Michael P. Stryker for critical reading of the manuscript. We also thank Hirofumi Ozeki and Srivatsun Sadagopan for helpful discussions. This work was supported by the National Institute of Health (R01 EY04726).

Accepted: October 4, 2010
Published: December 21, 2010

REFERENCES

Adesnik, H., and Scanziani, M. (2010). Lateral competition for cortical space by layer-specific horizontal circuits. Nature *464*, 1155–1160.

Alonso, J.M., and Martinez, L.M. (1998). Functional connectivity between simple cells and complex cells in cat striate cortex. Nat. Neurosci. *1*, 395–403.

Anderson, J., Lampl, I., Reichova, I., Carandini, M., and Ferster, D. (2000). Stimulus dependence of two-state fluctuations of membrane potential in cat visual cortex. Nat. Neurosci. *3*, 617–621.

Atallah, B.V., and Scanziani, M. (2009). Instantaneous modulation of gamma oscillation frequency by balancing excitation with inhibition. Neuron *62*, 566–577.

Azouz, R., and Gray, C.M. (2000). Dynamic spike threshold reveals a mechanism for synaptic coincidence detection in cortical neurons in vivo. Proc. Natl. Acad. Sci. USA *97*, 8110–8115.

Azouz, R., and Gray, C.M. (2003). Adaptive coincidence detection and dynamic gain control in visual cortical neurons in vivo. Neuron *37*, 513–523.

Azouz, R., and Gray, C.M. (2008). Stimulus-selective spiking is driven by the relative timing of synchronous excitation and disinhibition in cat striate neurons in vivo. Eur. J. Neurosci. *28*, 1286–1300.

Berens, P., Keliris, G.A., Ecker, A.S., Logothetis, N.K., and Tolias, A.S. (2008a). Comparing the feature selectivity of the gamma-band of the local field potential and the underlying spiking activity in primate visual cortex. Front. Syst. Neurosci. *2*, 2.

Berens, P., Keliris, G.A., Ecker, A.S., Logothetis, N.K., and Tolias, A.S. (2008b). Feature selectivity of the gamma-band of the local field potential in primate primary visual cortex. Front. Neurosci. *2*, 199–207.

Binzegger, T., Douglas, R.J., and Martin, K.A. (2004). A quantitative map of the circuit of cat primary visual cortex. J. Neurosci. *24*, 8441–8453.

Bokil, H., Purpura, K., Schoffelen, J.M., Thomson, D., and Mitra, P. (2007). Comparing spectra and coherences for groups of unequal size. J. Neurosci. Methods *159*, 337–345.

Bosking, W.H., Zhang, Y., Schofield, B., and Fitzpatrick, D. (1997). Orientation selectivity and the arrangement of horizontal connections in tree shrew striate cortex. J. Neurosci. *17*, 2112–2127.

Brainard, D.H. (1997). The psychophysics toolbox. Spat. Vis. *10*, 433–436.

Brette, R., Piwkowska, Z., Monier, C., Rudolph-Lilith, M., Fournier, J., Levy, M., Frégnac, Y., Bal, T., and Destexhe, A. (2008). High-resolution intracellular recordings using a real-time computational model of the electrode. Neuron *59*, 379–391.

Bringuier, V., Frégnac, Y., Baranyi, A., Debanne, D., and Shulz, D.E. (1997). Synaptic origin and stimulus dependency of neuronal oscillatory activity in the primary visual cortex of the cat. J. Physiol. *500*, 751–774.

Bringuier, V., Chavane, F., Glaeser, L., and Frégnac, Y. (1999). Horizontal propagation of visual activity in the synaptic integration field of area 17 neurons. Science *283*, 695–699.

Bruno, R.M., and Sakmann, B. (2006). Cortex is driven by weak but synchronously active thalamocortical synapses. Science *312*, 1622–1627.

Carandini, M. (2004). Amplification of trial-to-trial response variability by neurons in visual cortex. PLoS Biol. *2*, e264. 10.1371/journal.pbio.0020264.

Cardin, J.A., Palmer, L.A., and Contreras, D. (2005). Stimulus-dependent gamma (30–50 Hz) oscillations in simple and complex fast rhythmic bursting cells in primary visual cortex. J. Neurosci. *25*, 5339–5350.

Cardin, J.A., Palmer, L.A., and Contreras, D. (2007). Stimulus feature selectivity in excitatory and inhibitory neurons in primary visual cortex. J. Neurosci. *27*, 10333–10344.

Cardin, J.A., Carlén, M., Meletis, K., Knoblich, U., Zhang, F., Deisseroth, K., Tsai, L.H., and Moore, C.I. (2009). Driving fast-spiking cells induces gamma rhythm and controls sensory responses. Nature *459*, 663–667.

Churchland, M.M., Yu, B.M., Cunningham, J.P., Sugrue, L.P., Cohen, M.R., Corrado, G.S., Newsome, W.T., Clark, A.M., Hosseini, P., Scott, B.B., et al.

(2010). Stimulus onset quenches neural variability: A widespread cortical phenomenon. Nat. Neurosci. *13*, 369–378.

Das, A., and Gilbert, C.D. (1999). Topography of contextual modulations mediated by short-range interactions in primary visual cortex. Nature *399*, 655–661.

de la Rocha, J., Doiron, B., Shea-Brown, E., Josić, K., and Reyes, A. (2007). Correlation between neural spike trains increases with firing rate. Nature *448*, 802–806.

deCharms, R.C., and Merzenich, M.M. (1996). Primary cortical representation of sounds by the coordination of action-potential timing. Nature *381*, 610–613.

deCharms, R.C., and Zador, A. (2000). Neural representation and the cortical code. Annu. Rev. Neurosci. *23*, 613–647.

Douglas, R.J., Martin, K.A., and Whitteridge, D. (1991). An intracellular analysis of the visual responses of neurones in cat visual cortex. J. Physiol. *440*, 659–696.

Ecker, A.S., Berens, P., Keliris, G.A., Bethge, M., Logothetis, N.K., and Tolias, A.S. (2010). Decorrelated neuronal firing in cortical microcircuits. Science *327*, 584–587.

Engel, A.K., König, P., Gray, C.M., and Singer, W. (1990). Stimulus-dependent neuronal oscillations in cat visual cortex: Inter-columnar interaction as determined by cross-correlation analysis. Eur. J. Neurosci. *2*, 588–606.

Ferster, D., and Jagadeesh, B. (1992). EPSP-IPSP interactions in cat visual cortex studied with in vivo whole-cell patch recording. J. Neurosci. *12*, 1262–1274.

Finn, I.M., Priebe, N.J., and Ferster, D. (2007). The emergence of contrast-invariant orientation tuning in simple cells of cat visual cortex. Neuron *54*, 137–152.

Fries, P. (2009). Neuronal gamma-band synchronization as a fundamental process in cortical computation. Annu. Rev. Neurosci. *32*, 209–224.

Fries, P., Reynolds, J.H., Rorie, A.E., and Desimone, R. (2001). Modulation of oscillatory neuronal synchronization by selective visual attention. Science *291*, 1560–1563.

Gentet, L.J., Avermann, M., Matyas, F., Staiger, J.F., and Petersen, C.C. (2010). Membrane potential dynamics of GABAergic neurons in the barrel cortex of behaving mice. Neuron *65*, 422–435.

Gilbert, C.D. (1977). Laminar differences in receptive field properties of cells in cat primary visual cortex. J. Physiol. *268*, 391–421.

Gilbert, C.D., and Wiesel, T.N. (1989). Columnar specificity of intrinsic horizontal and corticocortical connections in cat visual cortex. J. Neurosci. *9*, 2432–2442.

Gray, C.M., and McCormick, D.A. (1996). Chattering cells: superficial pyramidal neurons contributing to the generation of synchronous oscillations in the visual cortex. Science *274*, 109–113.

Gray, C.M., and Singer, W. (1989). Stimulus-specific neuronal oscillations in orientation columns of cat visual cortex. Proc. Natl. Acad. Sci. USA *86*, 1698–1702.

Gray, C.M., König, P., Engel, A.K., and Singer, W. (1989). Oscillatory responses in cat visual cortex exhibit inter-columnar synchronization which reflects global stimulus properties. Nature *338*, 334–337.

Haider, B., Duque, A., Hasenstaub, A.R., and McCormick, D.A. (2006). Neocortical network activity in vivo is generated through a dynamic balance of excitation and inhibition. J. Neurosci. *26*, 4535–4545.

Hasenstaub, A., Shu, Y., Haider, B., Kraushaar, U., Duque, A., and McCormick, D.A. (2005). Inhibitory postsynaptic potentials carry synchronized frequency information in active cortical networks. Neuron *47*, 423–435.

Henrie, J.A., and Shapley, R. (2005). LFP power spectra in V1 cortex: the graded effect of stimulus contrast. J. Neurophysiol. *94*, 479–490.

Hubel, D.H., and Wiesel, T.N. (1962). Receptive fields, binocular interaction and functional architecture in the cat's visual cortex. J. Physiol. *160*, 106–154.

Jagadeesh, B., Gray, C.M., and Ferster, D. (1992). Visually evoked oscillations of membrane potential in cells of cat visual cortex. Science *257*, 552–554.

Jermakowicz, W.J., Chen, X., Khaytin, I., Bonds, A.B., and Casagrande, V.A. (2009). Relationship between spontaneous and evoked spike-time correlations in primate visual cortex. J. Neurophysiol. *101*, 2279–2289.

Kohn, A., and Smith, M.A. (2005). Stimulus dependence of neuronal correlation in primary visual cortex of the macaque. J. Neurosci. *25*, 3661–3673.

Lampl, I., Reichova, I., and Ferster, D. (1999). Synchronous membrane potential fluctuations in neurons of the cat visual cortex. Neuron *22*, 361–374.

Maldonado, P.E., Friedman-Hill, S., and Gray, C.M. (2000). Dynamics of striate cortical activity in the alert macaque: II. Fast time scale synchronization. Cereb. Cortex *10*, 1117–1131.

Maris, E., Schoffelen, J.M., and Fries, P. (2007). Nonparametric statistical testing of coherence differences. J. Neurosci. Methods *163*, 161–175.

Matsumura, M., Chen, D., Sawaguchi, T., Kubota, K., and Fetz, E.E. (1996). Synaptic interactions between primate precentral cortex neurons revealed by spike-triggered averaging of intracellular membrane potentials in vivo. J. Neurosci. *16*, 7757–7767.

Mitra, P., and Bokil, H. (2008). Observed Brain Dynamics (New York: Oxford University Press).

Monier, C., Chavane, F., Baudot, P., Graham, L.J., and Frégnac, Y. (2003). Orientation and direction selectivity of synaptic inputs in visual cortical neurons: A diversity of combinations produces spike tuning. Neuron *37*, 663–680.

Murthy, V.N., and Fetz, E.E. (1996). Synchronization of neurons during local field potential oscillations in sensorimotor cortex of awake monkeys. J. Neurophysiol. *76*, 3968–3982.

Nauhaus, I., Busse, L., Carandini, M., and Ringach, D.L. (2009). Stimulus contrast modulates functional connectivity in visual cortex. Nat. Neurosci. *12*, 70–76.

Niell, C.M., and Stryker, M.P. (2010). Modulation of visual responses by behavioral state in mouse visual cortex. Neuron *65*, 472–479.

Ohki, K., and Reid, R.C. (2007). Specificity and randomness in the visual cortex. Curr. Opin. Neurobiol. *17*, 401–407.

Ohki, K., Chung, S., Kara, P., Hübener, M., Bonhoeffer, T., and Reid, R.C. (2006). Highly ordered arrangement of single neurons in orientation pinwheels. Nature *442*, 925–928.

Okun, M., and Lampl, I. (2008). Instantaneous correlation of excitation and inhibition during ongoing and sensory-evoked activities. Nat. Neurosci. *11*, 535–537.

Okun, M., Naim, A., and Lampl, I. (2010). The subthreshold relation between cortical local field potential and neuronal firing unveiled by intracellular recordings in awake rats. J. Neurosci. *30*, 4440–4448.

Pelli, D.G. (1997). The VideoToolbox software for visual psychophysics: transforming numbers into movies. Spat. Vis. *10*, 437–442.

Perkel, D.H., Gerstein, G.L., and Moore, G.P. (1967). Neuronal spike trains and stochastic point processes. II. Simultaneous spike trains. Biophys. J. *7*, 419–440.

Pesaran, B., Pezaris, J.S., Sahani, M., Mitra, P.P., and Andersen, R.A. (2002). Temporal structure in neuronal activity during working memory in macaque parietal cortex. Nat. Neurosci. *5*, 805–811.

Poulet, J.F., and Petersen, C.C. (2008). Internal brain state regulates membrane potential synchrony in barrel cortex of behaving mice. Nature *454*, 881–885.

Priebe, N.J., and Ferster, D. (2008). Inhibition, spike threshold, and stimulus selectivity in primary visual cortex. Neuron *57*, 482–497.

Priebe, N.J., Mechler, F., Carandini, M., and Ferster, D. (2004). The contribution of spike threshold to the dichotomy of cortical simple and complex cells. Nat. Neurosci. *7*, 1113–1122.

Ray, S., and Maunsell, J.H. (2010). Differences in gamma frequencies across visual cortex restrict their possible use in computation. Neuron *67*, 885–896.

Sakata, S., and Harris, K.D. (2009). Laminar structure of spontaneous and sensory-evoked population activity in auditory cortex. Neuron *64*, 404–418.

Siegel, M., and König, P. (2003). A functional gamma-band defined by stimulus-dependent synchronization in area 18 of awake behaving cats. J. Neurosci. *23*, 4251–4260.

Smith, M.A., and Kohn, A. (2008). Spatial and temporal scales of neuronal correlation in primary visual cortex. J. Neurosci. *28*, 12591–12603.

Song, S., Sjöström, P.J., Reigl, M., Nelson, S., and Chklovskii, D.B. (2005). Highly nonrandom features of synaptic connectivity in local cortical circuits. PLoS Biol. *3*, e68. 10.1371/journal.pbio.0030068.

Tiesinga, P., Fellous, J.M., and Sejnowski, T.J. (2008). Regulation of spike timing in visual cortical circuits. Nat. Rev. Neurosci. *9*, 97–107.

Toyama, K., Kimura, M., and Tanaka, K. (1981a). Cross-correlation analysis of interneuronal connectivity in cat visual cortex. J. Neurophysiol. *46*, 191–201.

Toyama, K., Kimura, M., and Tanaka, K. (1981b). Organization of cat visual cortex as investigated by cross-correlation technique. J. Neurophysiol. *46*, 202–214.

Ts'o, D.Y., Gilbert, C.D., and Wiesel, T.N. (1986). Relationships between horizontal interactions and functional architecture in cat striate cortex as revealed by cross-correlation analysis. J. Neurosci. *6*, 1160–1170.

Tsodyks, M., Kenet, T., Grinvald, A., and Arieli, A. (1999). Linking spontaneous activity of single cortical neurons and the underlying functional architecture. Science *286*, 1943–1946.

Usrey, W.M., and Reid, R.C. (1999). Synchronous activity in the visual system. Annu. Rev. Physiol. *61*, 435–456.

Vinck, M., Lima, B., Womelsdorf, T., Oostenveld, R., Singer, W., Neuenschwander, S., and Fries, P. (2010). Gamma-phase shifting in awake monkey visual cortex. J. Neurosci. *30*, 1250–1257.

Volgushev, M., Pernberg, J., and Eysel, U.T. (2003). Gamma-frequency fluctuations of the membrane potential and response selectivity in visual cortical neurons. Eur. J. Neurosci. *17*, 1768–1776.

Volgushev, M., Chauvette, S., Mukovski, M., and Timofeev, I. (2006). Precise long-range synchronization of activity and silence in neocortical neurons during slow-wave oscillations. J. Neurosci. *26*, 5665–5672.

Yoshimura, Y., Dantzker, J.L., and Callaway, E.M. (2005). Excitatory cortical neurons form fine-scale functional networks. Nature *433*, 868–873.